ARTICLES

Luminescence Study of Water-Soluble CdS Nanoparticles Produced by Femtosecond Laser Ablation at High Laser Fluence

Weiwei Gong,[†,‡] Zhuhong Zheng,*[,†] Jinju Zheng,[†,‡] Wei Gao,[†,‡] Xuebing Hu,[†,‡] and Xinguang Ren[†]

Key Laboratory of Excited State Physics, Changchun Institute of Optics, Fine Mechanics and Physics, Chinese Academy of Sciences, 16 Eastern South-Lake Road, Changchun 130033, People's Republic of China and Graduate School of Chinese Academy of Sciences, Beijing 100049, People's Republic of China

Received: November 27, 2007; Revised Manuscript Received: March 24, 2008; In Final Form: April 10, 2008

Water-soluble CdS nanoparticles (NPs) with excellent colloidal stability were produced by femtosecond laser ablation at high laser fluence. The transmission electron microscope image of the obtained NPs exhibited a presence of two populations, characterized by low and high size dispersions, with different mean particle sizes. A comprehensive optical spectroscopy study of the NPs was carried out, and the results indicated a close correlation between the distribution properties and the luminescence characteristics. By analyzing the photoluminescence spectra of the CdS NPs synthesized under different focusing conditions, we revealed that the formation of the two-peak NPs distributions is related to the breakdown-induced plasma in water at such high laser fluence. However, this plasma-related ablation could manifest itself in the production of highly dispersed population, whereas the formation of the low-dispersed one is mainly attributed to the pure radiation-related ablation. This work will help us take advantage of the ultrapulse laser to synthesize favorable water-soluble semiconductors NPs for biosensing and labeling applications.

Introduction

Semiconductor nanocrystals (NCs), also known as quantum dots, have attracted much attention for their distinguished role in fundamental studies and technical applications, mainly due to their size-dependent properties and flexible processing chemistry.[1–3] These unique properties make them ideal probes applied in biology.[4–6] Toward this end, considerable efforts have been devoted to synthesizing high-quality water-soluble semiconductor NCs.[7–10] In recent years, the laser ablation technique has been developed as a successful physical method to fabricate semiconductor NCs.[11–16] This method allows easy control of the NCs size by optimizing the laser parameters and focusing conditions. Furthermore, crystalline phase transformations and contamination byproducts, which are usually observed for chemically reactive materials, can be avoided by carrying out the ablation in a controllable, contamination-free environment.

Femtosecond laser radiation has been getting more and more popular in recent years because of its efficiency in ablation of materials and effective control of particle size. Compared to laser ablation at relative long (e.g., nanosecond and picosecond) time scales, the use of a femtosecond laser can effectively minimize the laser-plume interaction and reduce the heat-affected zones.[16,17] Recent advances in laser ablation have utilized the synthesis of different materials in a liquid medium.[18–21] To make the NPs' growth more controllable, different sorts or different concentrations of surfactants have been used to reduce the NPs' size and prevent their further agglomeration. However, ionic surfactants could be problematic for further applications because of the unexpected nonband-edge luminescence or other biocompatibility problems.[21–25]

Alternatively, efficient size control approaches employ variations of physical parameters of femtosecond radiation, such as laser pulse energy, repetition rates, laser wavelength, focal spot size, focusing conditions, etc.[26–28] A popular method for size control in the recent research has been adjusting the laser fluence. It was demonstrated that small and well-dispersed NPs can be obtained in a liquid medium, and their mean size systematically increases with the increase in laser fluence. This can be well-explained by a radiation-related mechanism. However, when the laser ablation was carried out with large laser fluence, the NPs' growth appeared as a two-peak distribution. Therefore, some other mechanisms should be taken into account during the laser−matter interaction. We investigated the CdS NPs growth under different focusing conditions in water, and the ablation mechanisms were discussed accordingly. This will help us optimize laser parameters and focusing conditions to produce desired NPs.

Experimental Section

Laser ablation was carried out with a Ti/sapphire laser, which provided 100 fs full width at half-maximum (fwhm) pulses (wavelength 800 nm, maximum energy 1 mJ/pulse, repetition rate 1 kHz). The radiation was focused by an objective with a focal length of 5 cm and irradiated vertically to the target surface. A surface-polished CdS plate was fixed in the bottom

* To whom correspondence should be addressed. Fax: 86-431-86176320. E-mail: zhzheng1999@yahoo.com.cn.

† Changchun Institute of Optics, Fine Mechanics and Physics, Chinese Academy of Sciences.

‡ Graduate School of Chinese Academy of Sciences.

10.1021/jp711219e CCC: $40.75
Published on Web 06/14/2008

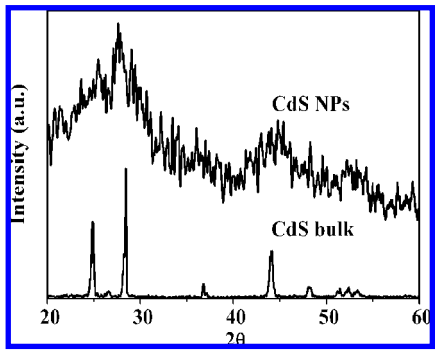

Figure 1. X-ray diffraction pattern of CdS NPs. The bulk CdS pattern corresponding to the wurtzite phase is also shown for comparison.

of a cuvette filled with deionized water. The cuvette was placed on a three-dimensional optical adjusting rack, which repetitively moved horizontally at a constant speed of 0.1 mm/s. The height of the water layer above the target surface was ~8 mm. The ablation was performed for 5 min with constant laser fluence (800 J/cm^2).

X-ray diffraction (XRD) data were collected on a Rigaku D/max-rA X-ray diffractometer using a Cu target radiation source. Absorption spectra were measured using a UV-3101PC UV−vis−NIR scanning spectrophotometer (Shimadzu). Room-temperature emission spectra were recorded on a Hitachi F-4500 spectrophotometer equipped with a 150-W Xe-arc lamp. Luminescence lifetime measurements were performed with an FL920 Fluorescence Lifetime spectrometer (Edinburgh Instruments) with MCP-PMT, in which the excitation light source was an NF900 ns flash lamp with 1 ns pulse duration. In addition, the morphology and distribution of the as-prepared samples were inspected with a transmission electron microscope (TEM, JEM-2010).

Results and Discussion

In our experiments, the laser ablation of CdS target in water was carried out under fixed laser fluence of 800 J/cm^2. When the laser irradiance was focused in the water, a plasma was formed near the focal point, which is due to the optical breakdown in water.[29] Then we placed the target at just beyond this plasma. (This target position was recorded as Z_1) It was found that a plume of the ejected material was produced, accompanied by the production of bubbles and a sharp sound. The sols became cloudy immediately and turned somewhat yellow. About an hour after the ablation, the obtained colloid was getting clear, and the colloidal NPs were found to be exceptionally stable for at least 9 months.

The XRD pattern of the obtained sample is shown in Figure 1. It can be seen that crystalline CdS NPs were obtained, in which all of the diffraction peaks can be index as hexagonal phase (JCPDS 02-0549) with the unit cell parameters $a_0 = b_0 = 4.142$ Å and $c_0 = 6.724$ Å. The peaks are getting broader as compared to the CdS bulk pattern, indicating the formation of nanocrystals. Figure 2 shows the TEM image of the obtained CdS NPs. The NPs are typically small (<10 nm), spheroidal, and nonagglomerated, and their distribution is characterized by a sharp peak at ~2 nm with a broad, slowly decreasing tail, as can be seen from Figure 2b. Such a distribution requires a superposition of two Gaussian functions, that is, a less dispersed population of particles with a mean size of 2.1 nm and a relatively broad, highly dispersed one with much larger mean particle size of ~5.0 nm.

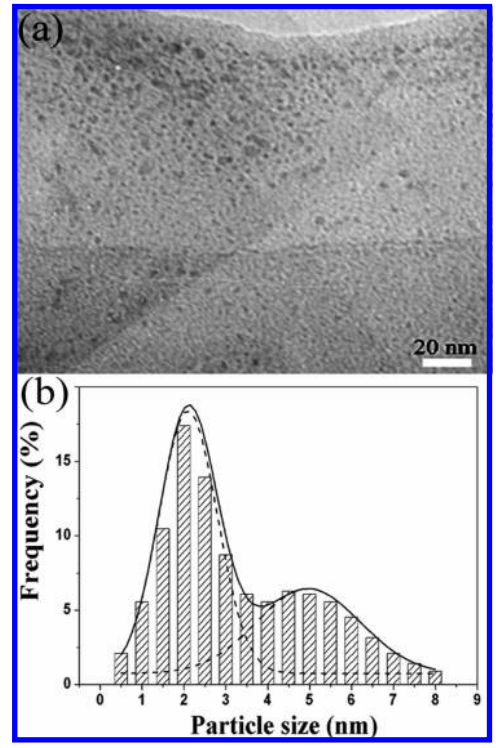

Figure 2. (a) TEM micrograph image and (b) corresponding size distribution of CdS nanoparticles prepared by femtosecond laser ablation in water.

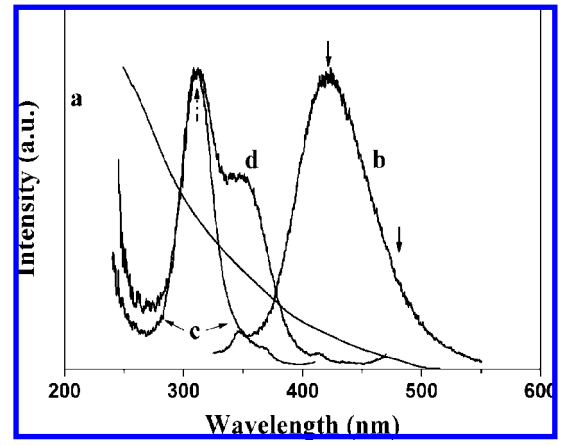

Figure 3. Summary of the spectroscopic data for CdS NPs. Absorption spectrum of CdS NPs as suspensions in water at room temperature is given in curve a. PL spectrum excited at 310 nm (denoted by dashed arrows) and photoluminescence excitation spectra monitored at 420 and 480 nm (denoted by solid arrows) are represented by curves b, c, and d. For clarity of presentation, the spectra are normalized.

Figure 3 presents a summary of the optical data for the sample. The room temperature absorption spectrum (curve a) shows an absorption onset of ~500 nm, which is considerably blue-shifted relative to the band gap energy of the bulk at ~2.42 eV (512 nm) for CdS, indicating the well-known phenomenon of quantum confinement. Hardly any obvious excitonic peak caused by the inhomogeneous size distribution of the NPs can be observed in the absorption spectrum. The PL spectrum excited at 310 nm (curve b) displays a high-energy peak of the excitonic peak centered on 420 nm with a long tail at a red wavelength down to 540 nm, as can be seen from Figure 3. The small-intensity peak observed at 347 nm is caused by Raman scattering of water at this excitation wavelength.[30] When monitoring the photoluminescence (PL) spectrum at 420 and

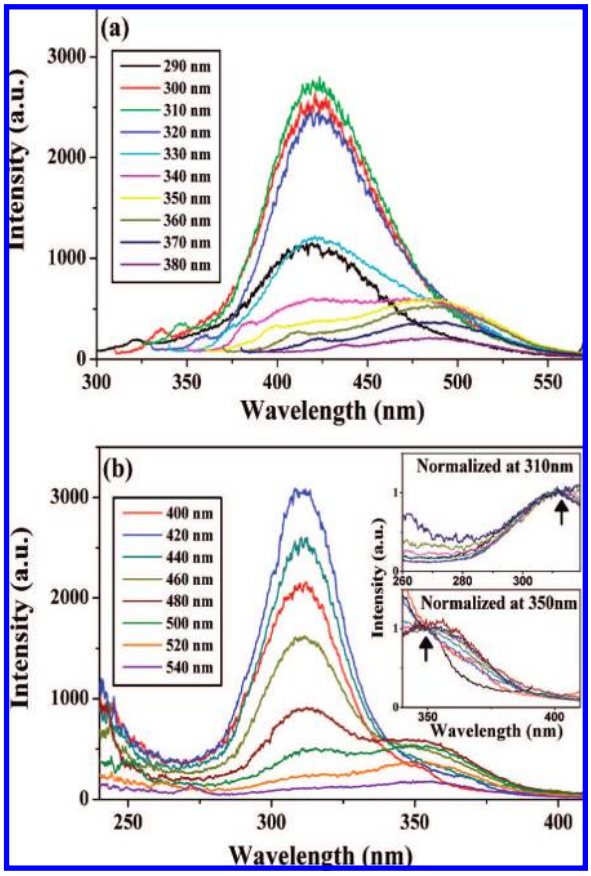

Figure 4. Wavelength dependence of room-temperature PL (a) and PLE (b) spectra of CdS NCs. Insert: the same spectra normalized at 310 (top) and 350 nm (bottom).

480 nm, two photoluminescence excitation (PLE) spectra were obtained and are shown as curves c and d, respectively. It was found that both the PLE spectra (curves c, d) have a peak at 310 nm; moreover, the spectrum monitored at 480 nm (curve d) has an extra peak at ~350 nm.

More detailed information is obtained by measuring the PL and PLE spectra at different excitation and detection energies, respectively. Figure 4a shows a series of PL spectra obtained at different excitation energies, starting from 4.3 eV (290 nm) going to lower energy with 10 nm steps until only the weak background signal could be detected. The series of PLE (Figure 4b) spectra were obtained in the same manner, changing the emission detection window from 2.3 eV (540 nm) up to 3.1 eV (400 nm) with 20 nm steps. It can be easily seen from Figure 4 that both the PL spectra and the PLE spectra of the CdS NPs have two peaks. Together with the presence of two-peak distribution of the CdS NPs in Figure 3, this correlation leads us to speculate that both of the peaks are due to excitonic recombination. On the basis of the quantum confinement,[31] we assign the high-energy peaks at ~2.95 eV (420 nm) to the less dispersed CdS NPs with mean particle size of 2.1 nm, and the low-energy excitonic peaks at ~2.59 eV (478 nm) to the highly dispersed NPs with mean size of 5.0 nm. For the PLE spectra, the two peaks are at 310 and 350 nm. The variety of the intensity with the detection energy of the two photoluminescence peaks indicates the absorption contribution to the band edge emission. Moreover, compared to the low-energy peak, the high-energy peak shows less dependence on the monitored PL wavelength during our detection window, indicating less dispersion of the NPs (see insets in Figure 4b).

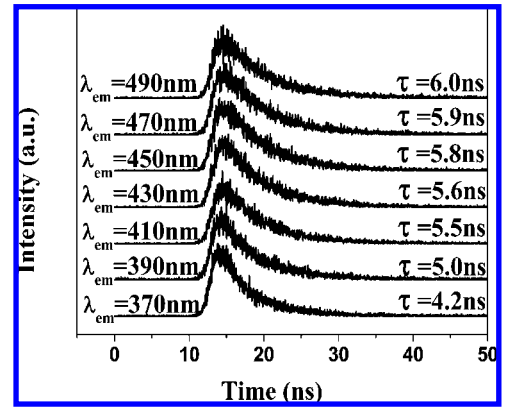

Figure 5. Room temperature luminescence decay as a function of emission wavelength for CdS NPs.

The spectral characteristics of the CdS NCs were further studied by the PL decay profiles as a function of monitoring wavelength. Figure 5 shows the room-temperature decay curves of the CdS NPs monitored from 370 to 490 nm with 20 nm steps. All these curves can be well-fitted by a single-exponential function. From the figure, we can see that the decay times decrease from 6.0 to 4.2 ns upon the shifting of the detection from 490 to 370 nm. The small change in PL lifetime suggests a similar recombination kinetic for the emission, which is commonly in accordance with excitonic transitions of different sizes of CdS NCs. On the other hand, the smaller particles, which have more types and numbers of quenching centers in the luminescence, arising from various surface defects,[32] would increase the nonradiative tunneling rate. Therefore, a shorter lifetime would be obtained for the small nanoparticles. Furthermore, a quantum size effect on the radiative recombination rate may be also attributed to the decrease in the lifetime.[33]

From the above discussion, we can see a close correlation between the distributed property and the PL characteristics. For the two populations of nanoparticles, the PL spectra present different excitonic peaks, and the wavelength dependence PL spectra gives a precise description of their distributions. In the following text, by analyzing the PL spectra of the samples synthesized at different target positions, we will have a discussion of the origin of the formation of the two-peak-distributed NPs.

As we know, when the femtosecond radiation acts on a target, the laser energy is simultaneously absorbed by electrons localized on the target surface. These electrons are subsequently induced avalanche ionization and optical breakdown, and then the microplasma plume is produced.[34,35]When the laser fluence is slightly above the ablation threshold, this radiation-related ablation is the dominant mechanism of the production of the plasma plume. In this case, the size of the NPs is completely controllable by adjusting the laser fluence, and the obtained NPs are well-dispersed. However, when the ablation was processed at high laser fluence in this study, it was found that two plasmas were presented during the ablation process. The first one is the microplasma plume, which ejects from the target surface, and the second one is the water breakdown-induced plasma, which is localized near the focal point and is much stronger. In this case, the NPs tend to present two peaks in their distributions. In our opinion, the formation of the two-peak distributed NPs is considerably related to the water breakdown-induced plasma.

To investigate the influence of the water breakdown-induced plasma to the size distribution, the ablations were carried out at three different target positions. The corresponding PL spectra

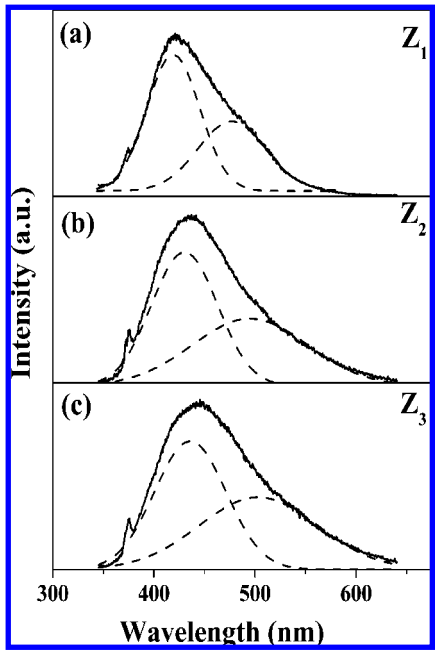

Figure 6. Photoluminescence spectra (excited at 330 nm wavelength) and fitted curves for the emission spectra of CdS NPs produced at different target positions: Z_1, Z_2, and Z_3.

TABLE 1: PL Emission and Fitted PL Components for CdS NPs Prepared at Different Target Positions

target position	description	fitted PL peaks	spectra width
Z_1	target, focal plane, plasma, z	A_1: 420 nm	0.36 eV
		B_1: 478 nm	0.38 eV
Z_2		A_2: 430 nm	0.45 eV
		B_2: 494 nm	0.58 eV
Z_3		A_3: 436 nm	0.47 eV
		B_3: 503 nm	0.59 eV

for the three samples were recorded and are shown in Figure 6. The results indicate that with the position of the target shifting from Z_1 to Z_3, the PL peak red-shifts from 422 to 445 nm, accompanied by a gradual increase in the spectral width. The spectra were well-fitted by two-peak Gaussian extrapolations. Detailed information is listed in Table 1.

As we can see from the Table, the relatively high energy PL peak red-shifts from 420 to 436 nm, accompanied by a gradual increase in the spectral width from 0.36 to 0.47 eV, with the reduction of the relative distance between the target surface and the focal plane. The low-energy one shifts from 478 to 503 nm, with an increasing spectrum width from 0.38 to 0.59 eV. Consistent with the expected shift due to the quantum confinement, it is easy to find that the highly dispersed population has a larger shift of the mean size as well as its distribution as compared to the less dispersed one. Consequently, we can conclude that the highly dispersed population has been significantly influenced by the water breakdown-induced plasma during the ablation. According to ref 29, the occurrence of the optical breakdown phenomenon could absorb up to 70% of the laser power. In our view, this energy is high enough to cause additional ablation of the material during the process. Therefore, with the elimination of the distance between the target and the focal plane, the plasma energy deposited on the target surface was increased. As a result, relatively large NPs with broad distributions were produced. These results agree well with the recent report in ref 28. In addition, possible mechanisms of the plasma-related ablation of material could be target heating by the plasma or its erosion through the collapse of the cavitation bubble.[16,28,29]

On the other hand, the production of the less dispersed NPs, which have fewer responses to the water breakdown-induced plasma, is associated with the pure radiation-based ablation of nanoclusters and their subsequent coalescence in the water environment. In our view, this pure radiation-based ablation can be explained as follows. When it is assumed that the ultrashort laser pulse has a Gaussian beam profile, the laser fluence can be written as

$$F(r,z) = F_0 \exp\left\{-2\left[\frac{r}{\omega(z)}\right]^2\right\} \quad (1)$$

where $\omega(z)$ is the beam diameter depending on the position and the lateral position r where the fluence exceeds the ablation threshold can be calculated.[36] F_0 is the normalized value so that its surface integration gives the total energy of the laser pulse

$$U = (1/2)F_0\pi\,\omega(z)^2 \quad (2)$$

Under fixed laser energy, the changing of the target position (z) with respect to the objective focal plane results in the variety of the laser fluence for ablation. In our experiments, the shift of the target position from Z_1 to Z_3 corresponds to an increase in the laser fluence, which in turn broadens the size distribution of the NPs, and the inherent inhomogeneous broadening of the PL spectra, due mainly to the variance in nanoparticle sizes, gets larger.

Conclusion

We have revealed the presence of two-peak size distributed water-soluble CdS NPs prepared by femtosecond laser ablation of a bulk CdS target at high laser fluence. A TEM image and a comprehensive optical spectroscopy study were used to characterize the obtained NPs. The experimental results indicate a close correlation between the distribution and luminescence properties of the sample. On the basis of this correlation, we have showed that with the target shifting toward the focal plane, the mean particle sizes of the two populations were increased, and the size distributions were broadened, as well. Furthermore, the less dispersed population exhibited fewer responses to the plasma than the highly dispersed one. It is probably because the less dispersed NPs primarily originated from the radiation-related ablation of material, whereas the highly dispersed population is mainly attributed to the plasma-related ablation. Finally, we suggest here that the plasma-related ablation tends to cause some large particles and relative broad distributions. Therefore, to synthesize favorable water-soluble semiconductor NPs, we should eliminate the influence of the plasma−matter interaction by avoiding the water breakdown-induced plasma or carrying out the ablation at low laser fluence.

References and Notes

(1) Bawendi, M. G.; Steigerwald, M. L.; Brus, L. E. *Annu. Rev. Phys. Chem.* **1990**, *41*, 477.
(2) Alivisatos, A. P. *Science* **1996**, *271*, 933.

(3) Murray, C. B.; Norris, D. J.; Bawendi, M. G. *J. Am. Chem. Soc.* **1993**, *115*, 8706.
(4) Chan, W. C. W.; Nie, S. M. *Science* **1998**, *281*, 2016.
(5) Bruchez, M.; Moronne, M.; Gin, P.; Weiss, S.; Alivisatos, A. P. *Science* **1998**, *281*, 2013.
(6) Tessler, N.; Medvedev, V.; Kazes, M.; Kan, S. H.; Banin, U. *Science* **2002**, *295*, 1506.
(7) Zhao, H.; Douglas, E. P.; Harrison, B. S.; Schanze, K. S. *Langmuir* **2001**, *17*, 8428.
(8) Gubin, S. P.; Kosobudskii, J. D. *Russ. Chem. Rev.* **1983**, *52*, 766.
(9) Murray, C. B.; Norris, D. J.; Bawendi, M. G. *J. Am. Chem. Soc.* **1993**, *115*, 8706.
(10) Petit, C.; Lixon, P.; Pileni, M. P. *J. Phys. Chem.* **1993**, *97*, 12974.
(11) Usui, H.; Shimizu, Y.; Sasaki, T.; Koshizaki, N. *J. Phys. Chem. B* **2005**, *109*, 120.
(12) Burnin, A.; Sanville, E.; BelBruno, J. J. *J. Phys. Chem. A* **2005**, *109*, 5026.
(13) Sylvestre, J.-P.; Poulin, S.; Kabashin, A. V.; Sacher, E.; Meunier, M.; Luong, J. H. T. *J. Am. Chem. Soc.* **2004**, *126*, 7176.
(14) Murali, A.; Barve, A.; Leppert, V. J. ; Risbud, S. H.; Kennedy, I. M.; Lee, H. W. H. *Nano. Lett.* **2001**, *1*, 287.
(15) Mafune, F.; Kohno, J.-Y.; Takeda, Y.; Kondow, T. *J. Phys. Chem. B* **2002**, *106*, 7575.
(16) Kabashina, A. V.; Meunier, M. *J. Appl. Phys.* **2003**, *94*, 7941.
(17) Chin, A. H.; Schoenlein, R. W.; Glover, T. E. *Phys. Rev. Lett.* **1999**, *83*, 336.
(18) Said, A.; Sajti, L.; Giorgio, S.; Marine, W. *J. Phys.: Conf. Ser.* **2007**, *59*, 259.
(19) Ruth, A. A.; Young, J. A. *Colloids Surf. A* **2006**, *279*, 121.
(20) Zeng, H. B.; Cai, W. P.; Hu, J. L.; Duan, G. T.; Liu, P. S.; Li, Y. *Appl. Phys. Lett.* **2006**, *88*, 171910.
(21) Gong, W. W.; Zheng, Z. H.; Zheng, J. J.; Hu, X. B.; Gao, W. *J. Appl. Phys.* **2007**, *102*, 064304.
(22) Zhou, H. S.; Honma, I.; Komiyama, H.; Haus, J. W. *J. Phys. Chem.* **1993**, *97*, 895.
(23) Peng, X. G.; Schlamp, M. C.; Kadavanich, A. V.; Alivisatos, A. P. *J. Am. Chem. Soc.* **1997**, *119*, 7019.
(24) Hoheisel, W.; Colvin, V. L.; Johnson, C. S.; Alivisatos, A. P. *J. Chem. Phys.* **1994**, *101*, 8455.
(25) Choi, S. H.; Sasaki1, T.; Shimizu, Y.; Yoon1, J. W.; Nichols, W. T.; Sung, Y. E.; Koshizaki, N. *J. Phys.: Conf. Ser.* **2007**, *59*, 388.
(26) Nichols, W. T.; Sasaki, T.; Koshizaki, N. *J. Appl. Phys.* **2006**, *100*, 114912.
(27) Gruzdev, V. E.; Gruzdeva, A. S. *Proc. SPIE* **2001**, *4423*, 295.
(28) Korte, F.; Nolte, S.; Chichkov, B. N.; Bauer, T.; Kamlage, G.; Wagner, T.; Fallnich, C.; Welling, H. *Appl. Phys. A: Mater. Sci. Process.* **1999**, *69*, S7.
(29) Vogel, A.; Noack, J.; Nahen, K.; Theisen, D.; Busch, S.; Parlitz, U.; Hammer, D. X.; Noojin, G. D.; Rockwell, B. A.; Birngruber, R. *Appl. Phys. B: Laser Opt.* **1999**, *68*, 271.
(30) Vallee, P.; Lafait, J.; Ghomi, M.; Jouanne, M.; Morhange, J. *J. Mol. Struct.* **2003**, *651*, 371.
(31) Lippens, P. E.; Lannoo, M. *Phys. Rev. B* **1989**, *39*, 10935.
(32) O'Neil, M.; Marohn, J.; McLendon, G. *J. Phys. Chem.* **1990**, *94*, 4356.
(33) Chestnoy, N.; Harris, T. D.; Hull, R.; Brus, L. E. *J. Phys. Chem.* **1986**, *90*, 3393.
(34) Ready, J. F. ; Farson, D. F., Eds. *LIA Handbook of Laser Materials Processing*; Springer: Heidelberg, 2001.
(35) Lorazo, P.; Lewis, L. J.; Meunier, M. *Phys. Rev. Lett.* **2003**, *91*, 225502-1.
(36) Obara, M.; Yabe, H.; Hirayama, Y.; Takahashi, K.; Furusawa, K.; Barnier, F. *Proc. SPIE* **2000**, *4065*, 210.

JP711219E